INNSPUB
Journal of Biodiversity and Environmental Sciences (JBES)
ISSN: 2220-6663 (Print) 2222-3045 (Online)
Vol. 23, No. 6, p. 110-120, 2023
http://www.innspub.net

RESEARCH PAPER OPEN ACCESS

Solar driven photocatalytic activities of metal oxide/ biopolymer nanocomposites upon methylene blue dye

T. Uma Rajalakshmi[*1], S. Amutha[2], S. Rajaduraipandian[3], E. Pushpalakshmi[2], G. Annadurai[*2]

[1]*P.G & Research Department of chemistry, Rani Anna Government College for Women, Manonmaniam Sundaranar University, Tirunelveli, India*

[2]*Sri Paramakalyani Centre of Excellence in Environmental Sciences, Manonmaniam Sundaranar University, Alwarkurichi, India*

[3]*Sri Paramakalyani College, Manonmaniam Sundaranar University, Alwarkurichi, India*

Article published on December 14, 2023

Key words: Biopolymers, Car boxy methyl cellulose, Nano composites, Sodium alginate, Zinc oxide

Abstract

The present investigation aims to synthesize, characterize, and study the photocatalytic activities of zinc oxide/biopolymer nanocomposites. Sodium alginate and carboxy methyl cellulose were the biopolymers used. A simple precipitation method was adopted for the synthesis. The zinc oxide nanoparticles were calcined at 550°C for 2 hours in a muffle furnace and then mixed with the respective biopolymers under proper proportions and the resulting mixtures were poured in an autoclave maintained at 180°C for 12 hours, filtered, washed and dried at 60°C for 2 hours. The synthesized nanocomposites were characterized using XRD, SEM, TEM, FTIR, UV-VIS and AFM. The photocatalytic activities of the nanocomposites were tested using methylene blue dye under different experimental conditions by varying the pH, catalytic dosage, concentration of the dye and contact time. Excellent photocatalytic degradation of the dye was achieved under direct sunlight irradiation for both nanocomposites.

***Corresponding Author:** T. Uma Rajalakshmi ✉ rajiumaselva@gmail.com

Introduction

Nanotechnology is the science and engineering of ceramics or crystalline materials, glasses or non-crystalline materials, polymers or long molecular chain materials and metals or cohesively bonded materials (HoltzJ *et al.,* 1997). During the last decades semiconductor-assisted photocatalytic oxidation processes have received considerable attention due to their potential application in photocatalysis, environmental remediation, self-cleaning and bactericidal coatings, new generation solar cells, hydrogen production and sensing. In this perspective, TiO_2 and ZnO represent the most widely used photocatalyst due to its high chemical stability, commercial availability and excellent catalytic properties (Hengyu Xu *et al.,* 2022; Redouane Haounati *et al.,* 2023).

Interestingly, nanocomposite materials offer the opportunity to incorporate in the same host matrix multiple functions deriving from distinct types of nanocatalysts such as semiconductor nanoparticles (NPs) (i.e. TiO_2 or ZnO), metals, carbon nanotubes and graphene. The range of wavelength needed for photocatalysis to the visible region, to make them re-coverable by using magnetic field or to increase their efficiency by enhancing the lifetime of the electron-hole pair. (ZnO), copper oxide (CuO) (Liu *et al.,* 2004a; Jiang *et al.,* 2002; Lin *et al.,* 2004), nickel oxide (NiO) (Hagfeldt *et al., 2001*; Liu *et al., 2004b*; Nuli *et al.,* 2003) gallium oxide (Ga_2O_3) (*Dai et al.,* 2002; Changhyun *et al.,* 2012) etc. Water contamination becomes a severe issue because 2% of dyes produced from different industries are discharged directly to aqueous effluents (Rauf *et al.,* 2009).

They create severe environmental problems due to organic and inorganic chemicals in them. It drags the attention of many researchers due to potentially carcinogenic pollutants in contaminated water. So, it is necessary to remove colored dyes before discharging them into the environment (Pearce *et al.,* 2003; Robinson *et al.,* 2001). Therefore, its removal from the polluted water is of significant importance. Many proposed methods of environmental decontamination involve the oxidation of organic pollutants. However, one of the main challenges is to incorporate photocatalytic nanomaterials in properly designed host polymers, for instance hybrid inorganic-organic and fluorinated polymers, since photocatalysts can degrade any organic material, and thus also the organic matrix in which the NPs are embedded. The overarching goal of this work is to provide a critical study of current research on the applications of Metal oxide/Biopolymer Nanocomposites on the integrated adsorptive and photocatalytic removal of dyestuff in the environment.

Material methods

Zinc Nitrate, Ammonium Carbonate, Sodium Alginate and Ethanol were availed from Merck, India Pt. Ltd. Deionised water was used throughout the reaction process. All the reagents used in this study were of analytical grade.

Preparation of Zincoxide Nanoparticle

The Zn $(NO_3)_2$ solutions (1.5 mol/L) was slowly dropped into the $(NH_4)_2CO_3$ solution (2.25 mol/L) with vigorous stirring. Then the precipitate derived from the above reaction was collected by filtration and rinsed three times with high-purity water followed by ethanol. Subsequently the washed precipitate was dried at 80°C to form the precursor Zincoxide. Finally, the precursor was calcined at a temperature of 550°C for 2 hrs in the muffle furnace (Changchunchen *et al.,* 2008) to obtain the Nano-sized Zincoxide particles.

Preparation of Photocatalytic Nanocomposite Materials

The precursor Zinc oxide nanoparticle is mixed with 100ml of solution containing biopolymers sodium alginate and carboxyl methyl cellulose under proper proportions and stirred uniformly for about 6 hours. The resulting mixtures are poured in an autoclave coated with Teflon lining maintained at 180°C for 12 hours, filtered, washed with ethanol and water and dried at 80°C for 2 hours. The synthesized nanocomposite was characterised by XRD, SEM, TEM, FTIR and AFM were investigated.

Results and discussion

X-ray diffraction

X-ray diffraction pattern is used to confirm the purity, phase, average particle size and overall crystallinity of the synthesized nanocomposites. Fig. 1 shows the XRD patterns of a. precursor ZnO b. ZnO / SA and c. ZnO /cmC nanocomposites. The peaks at 2θ = 31°, 34°, 36°, 47°, 56°, 62°, 67° and 69° of Zinc oxide/ sodium alginate nanocomposites are corresponding to (100), (002), (101), (102), (110), (103), (112) and (201) in the JCPDS data card 89-0510. Hexagonal structure of zinc oxide was confirmed by the (1 0 1) crystalline peak and the average crystal size of synthesized ZnO / SA nanoparticle is calculated to be 43 nm. The presence of sodium alginate as well as characteristic reflections indicated the maintenance of the sodium alginate and Zinc oxide nanoparticles in crystallographic organization of the nanocomposites. The presence of high and narrow shaped peaks highlights that Zinc oxide nanoparticles possess high crystallinity and low surface defects (Lupan *et al., 2010;* (Uma Rajalakshmi and Alagumuthu, 2019; 2021) and were of ultrapure phase and the XRD for ZnO /cmC nanocomposites (JCPDS file no. 36-1451) as shown in the fig c, confirms that the synthesized nanocomposites have wurtzite hexagonal structure with high purity. The different peak orientations were observed along the (100), (002), (101), (102) and (110) planes which is in good agreement with the intrinsic fundamental structure of zinc oxide as reported in the literature and the particle size was calculated to be 41 nm.

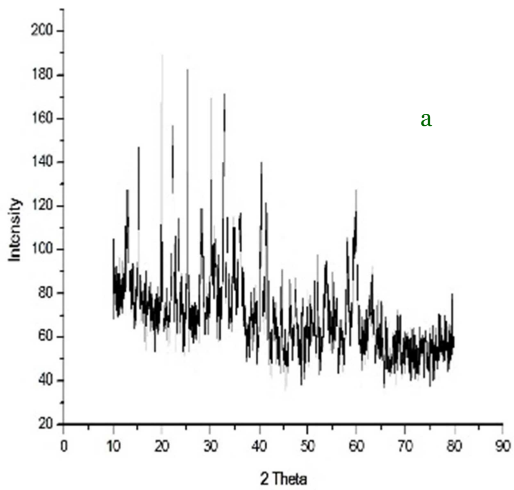

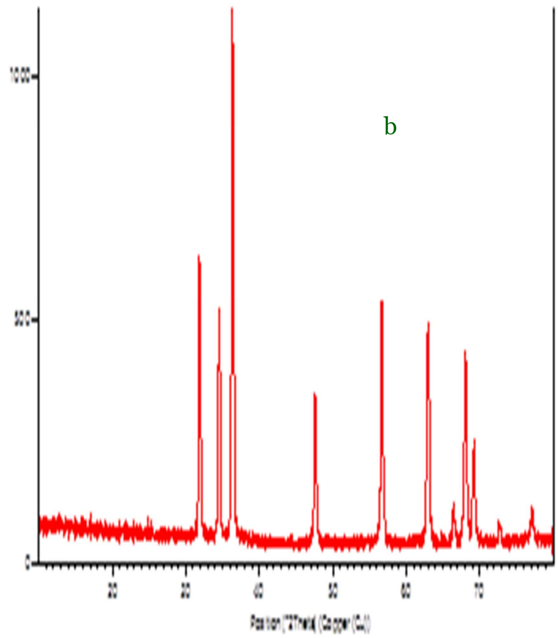

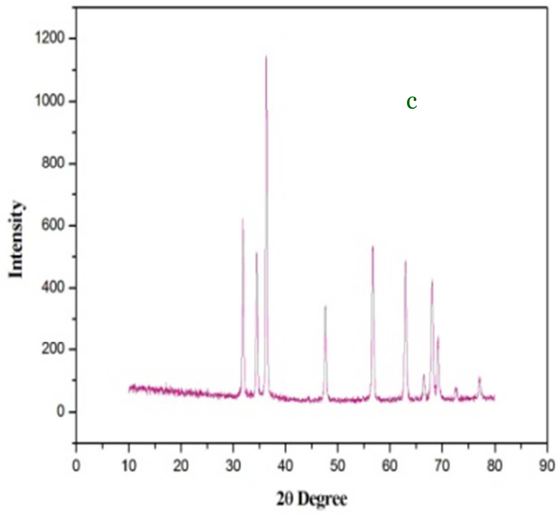

Fig. 1. The XRD patterns of a. precursor ZnO b. ZnO/SA c. ZnOcmC.

Scanning Electron Microscopy

SEM was used to study the surface morphology of the synthesized nanocomposites. This image was proved to confirm the structural morphology of the synthesized a. ZnO/ SA nanocomposite and b. ZnO /cmC nanocomposite. Fig 2 depicts the uniform distribution of roughly spherical shaped ZnO into the SA andcmC biopolymer matrices. It is observed that ZnO particles are surrounded by the bio polymer matrix hence it appears as agglomerated macromolecules (Raizada *et al., 2014*; Byrappa *et al., 2006*; Sobana *et al.,* 2007).

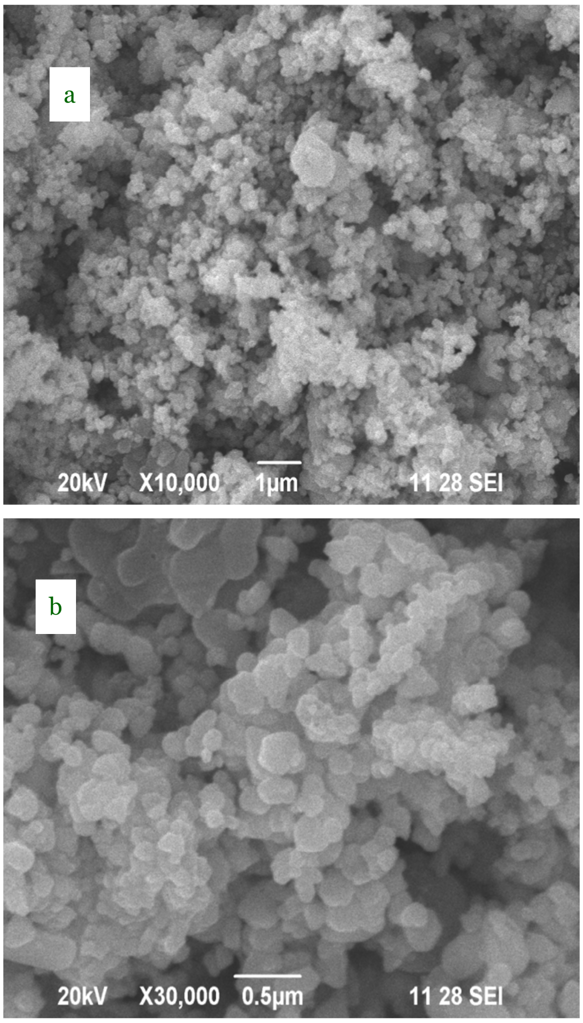

Fig. 2. The structural morphology of the synthesized a. ZnO/ SA nanocomposite and b. ZnO /cmC nanocomposite

Transmission Electron Microscopy

Fig. 3 shows the TEM image of the prepared a. ZnO/ SA and b. ZnO /cmC nanocomposites. The size of the particle observed in the TEM image is in the range of 40-45nm which is in the good agreement with that calculated using Debye–Scherrer formula. The shape of the nanoparticles is in accordance with the hexagonal wurtzite structure of ZnO which are homogeneously dispersed in the biopolymer matrix.

After composite formation, ZnO nanoparticles were found to be entrapped in the biopolymer matrix. Therefore, the nanoparticles were not simply mixed up or blended with the bio-polymer; they were rather bound by the bio-polymer chain (Vinayagam *et al.,* 2018; Chen *et al.,* 2014).

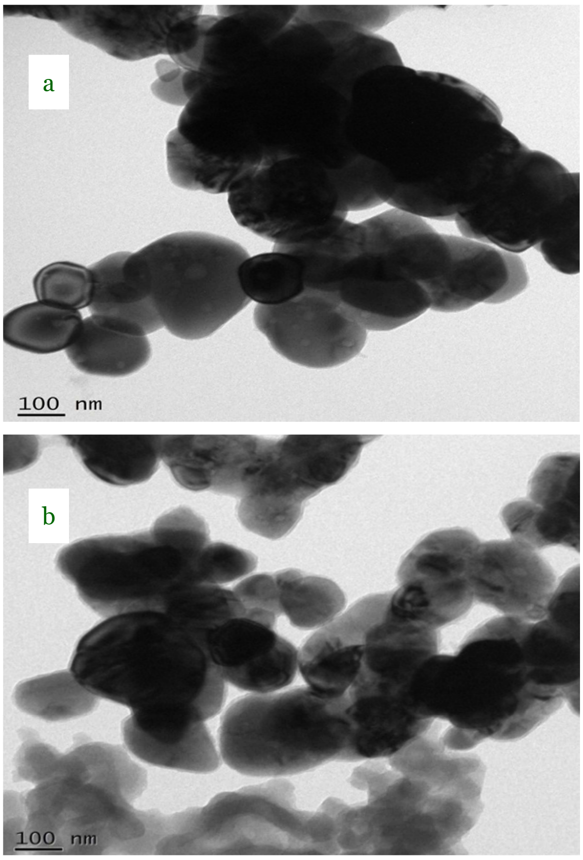

Fig. 3. The TEM image of the prepared a. ZnO/ SA and b. ZnO /cmC nanocomposite

Fourier transforms infrared spectroscopy

Fourier transform infrared spectroscopy (FTIR) data of the a. ZnO/ SA and b. ZnO /cmC nanocomposites are represented in the Fig 4. The infrared absorption measurements are carried out to characterize the nanocomposites potential interactions. In the fig a. the absorption band characteristic of alginate were observed at 3448cm^{-1} corresponding to OH group and the peaks near 1637cm^{-1} 1543cm^{-1} and 1460cm^{-1} assigned to symmetric and asymmetric stretching vibration of COO^{--} groups, respectively (Dang *et al.,* 2018*;* Uma Rajalakshmi and Alagumuthu, 2019; 2021). The band around 1100cm^{-1} (C-O-O) stretching) were attributed to its saccharide structure. The absorption band around 1738cm^{-1} may be attributed to the C-O stretching of the lactone. The broadening of the peak at 3448cm^{-1} could be due to intermolecular hydrogen bonding between ZnO and alginate molecules. In the fig b. the vibrational mode at 438cm^{-1} corresponds to Zn-O absorption in the hexagonal type ZnO. The characteristic band at

3431cm^{-1} corresponds to the stretching vibration of O-H groups. The presence of other band at 1384cm^{-1} is probably due to the carbonate moieties which is generally observed when FT-IR samples are measured in air (Lili *et al.*, 2006). Vibrational mode observed at 2854 and 2924cm^{-1} is due to C-H stretching vibration. ThecmC displays a broad peak at 1628cm^{-1}corresponding to stretching vibration of C=O of (COOH) group.

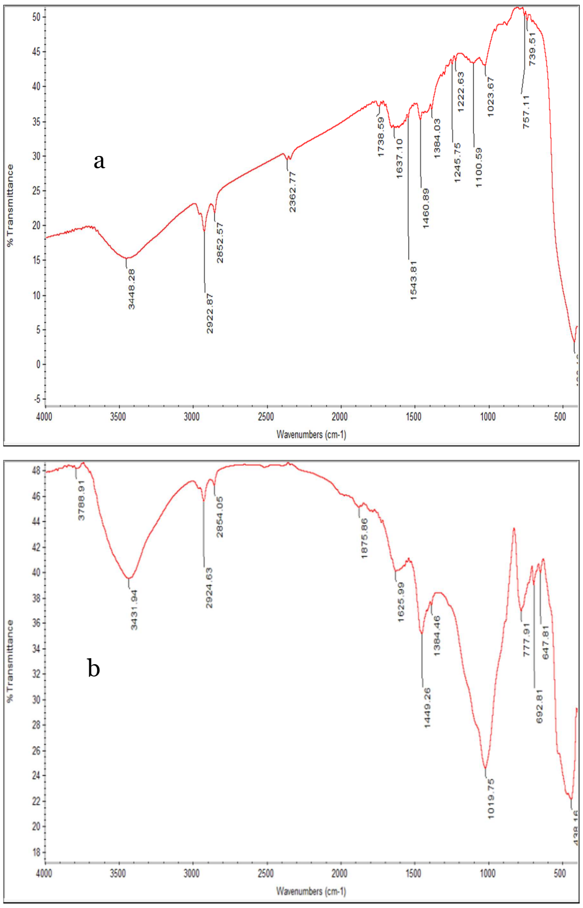

Fig. 4. Fourier transform infrared spectroscopy (FTIR) data of the a. ZnO/ SA and b. ZnO /cmC nanocomposite

UV-VIS absorption spectra

The room temperature UV-vis absorption spectra of ZnO / SA and ZnO /cmC nanocomposites are shown in Fig. 5 a and b. The nanocomposites were dispersed in ethanol with a concentration of 0.1% wt. and then the solutions were used to perform the UV-vis measurement. The spectra reveal a characteristic absorption peak of zinc oxide at a wavelength of 330 nm which can be assigned to the intrinsic band-gap absorption of zinc oxide due to the electron transitions from the valence band to the conduction band (O2p → Zn3d) (Byrappa *et al.,* 2006; Sobana *et al.,* 2007; (Uma Rajalakshmi and Alagumuthu, 2019; 2021*)*. In addition, this sharp peak shows that the particles are in nanosized, and the particle size distribution is narrow.

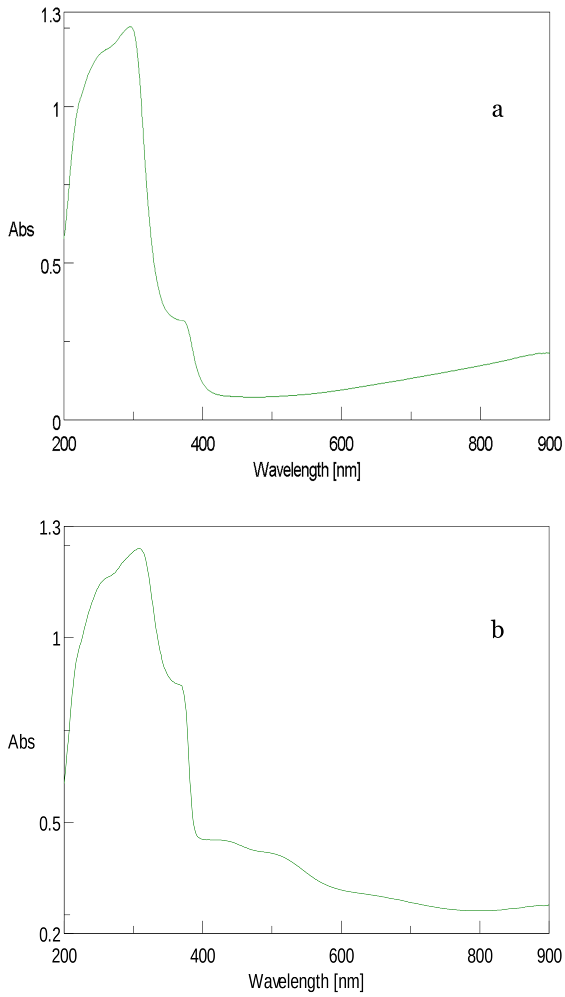

Fig. UV-Vis absorption spectra of a.ZnO / SA b. ZnO /cmC nanocomposite

Atomic Force microscope

Surface topology of the synthesized nanocomposites were studied by Atomic Force microscope (AFM) analysis as shown in Fig. 6 a and b. The results showed a uniform surface and indicated that the particles have uniform dimensions and maximum surface particle size of the ZnO / biopolymer nanocomposites are within 45 nm. Roughness, porosity and particle dimension were evaluated by AFM image (Thi and Lee, 2017; Chen *et al.,* 2016).

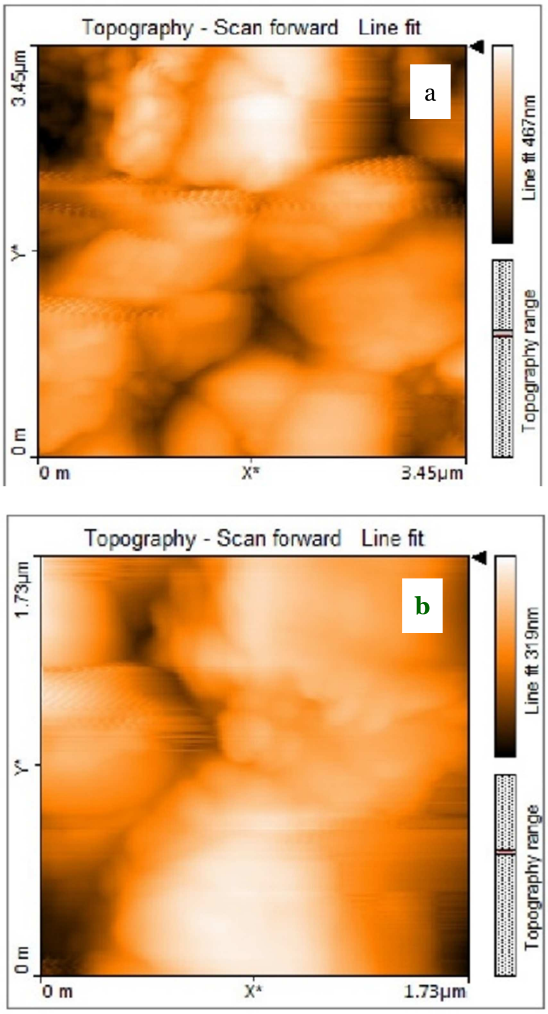

Fig. 6. AFM images of a. ZnO / SA b. ZnO /cmC.

Photocatalytic degradation studies

The photocatalytic activities is evaluated by the degradation of MB dye in aqueous solution under sunlight using ZnO /SA and ZnO /cmC nanocomposites which were used as photocatalysts for the decomposition of the MB dye by the hydroxyl radicals formed at their interface.

The absorption of MB dye at 664 nm was chosen to monitor the photocatalytic degradation process. Dye degradation was visually detected by gradual change in the color from deep blue to colorless solution.

The dye degradations in the presence of synthesized ZnO / SA and ZnO /cmC nanocomposites were verified by the decrease of the peak intensity at 664 nm during 120 min exposure in sunlight shown in Fig.7 a and b. The enhanced photocatalytic performance in the case of the synthesized nanocomposite is attributed to the synergistic effects between ZnO nanoparticles and biopolymers which can decrease the rate of recombination of electron-hole pairs caused by the trapping of excited electrons from the conduction band of ZnO nanoparticles (Thi and Lee, 2017; Chen *et al.*, 2016; Yang *et al.*, 2018a; Melián *et al.*, 2009; Raizada *et al.*, 2014; Byrappa *et al.*, 2006; Sobana *et al.*, 2007; Vinayagam *et al.*, 2018; Chen *et al.*, 2014).

It has been reported that their photocatalytic activity relies on the particle size, phase structure, adsorption capability, and e^-/h^+ recombination rate (Yang *et al.*, 2018b; (Uma Rajalakshmi and Alagumuthu, 2019; 2021). The kinetic plot of ln (A/A0) versus time (T) shows a linear graph in Fig.8 which suggests that the degradation follows a first order kinetics with a linear regression coefficient (R^2) 0.988.

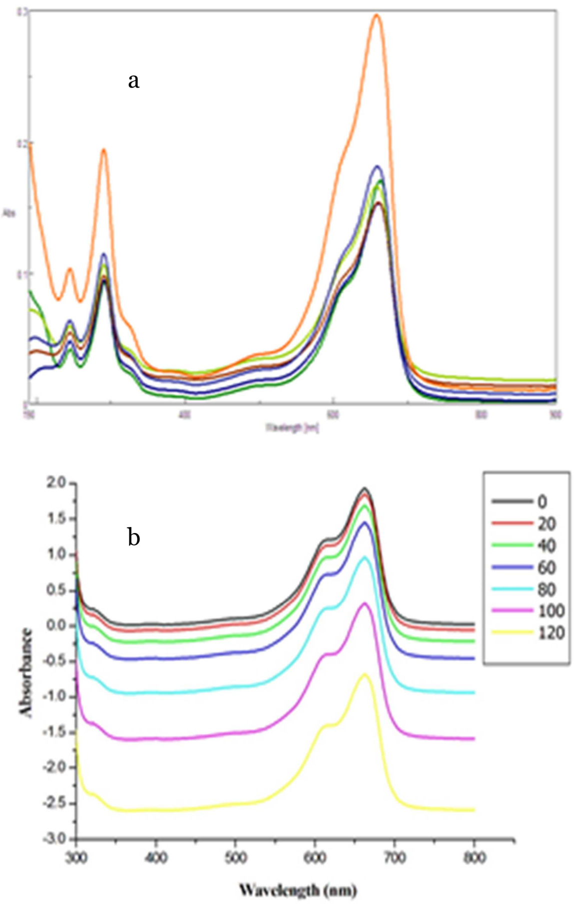

Fig.7. UV-Vis spectra of MB dye treated under photocatalytic reaction in the presence of a. ZnO / SA and b. ZnO /cmC.

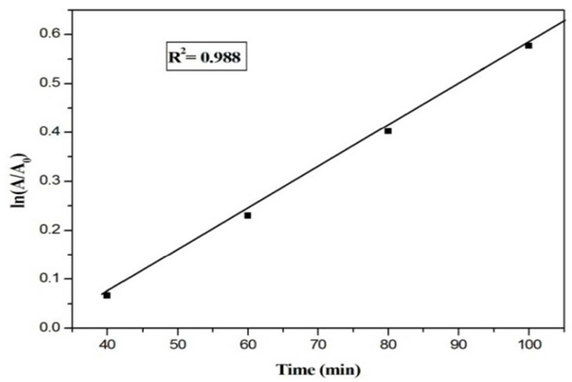

Fig. 8. The photocatalytic degradation of MB dye and kinetics fit for the degradation..

Effect of catalyst loading

The percentage removal of the MB dye was found to vary linearly with increase in the dose of the catalyst (10-50)mg for a. ZnO / SA and 10-20mg for b. ZnO /cmC) indicating the heterogeneous regime as shown in Fig.9. a and b. This may probably be due to: (i) increase in the extent of dye adsorption on the catalyst surface; (ii) increase in the number of surface-active sites; (iii)enhanced generation of hydroxyl radicals due to increase in the concentration of charge carriers (Baran *et al.,* 2008; Neppolian *et al.,* 2002 (Uma Rajalakshmi and Alagumuthu, 2019; 2021).

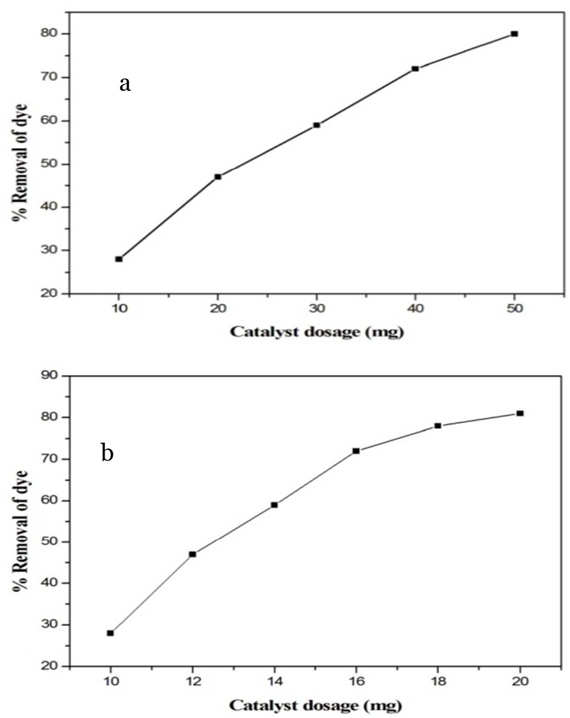

Fig. 9. Variation of % removal of the dye against catalyst loading for a.ZnO / SA and b. ZnO /cmC.

Effect of initial concentration of dye

The initial concentration of the MB dye with constant catalytic loading (50mg/50mlfor ZnO / SA and 20mg/50ml for ZnO /cmC) was varied from 10ppm to 50ppm. It was observed that the rate constant decreases from 10ppm to 50ppm dye concentration. This is due to the fact that more dye molecules are available in the photoactive volume for the degradation process. Rate constant decreases with further increase in concentration of dye above the optimal value. The decrease is attributed to the fact that the dye itself will start acting as a filter for the incident irradiation, reducing the photoactive volume. At low concentrations, the reverse effect is observed (Kudo and Miseki, 2009; Uma Rajalakshmi and Alagumuthu, 2019; 2021), as shown in Fig.10 a and b.

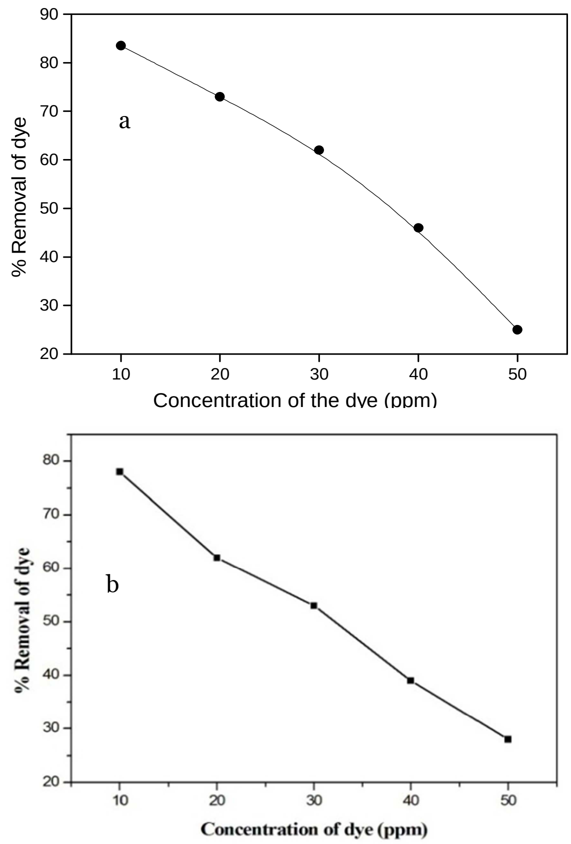

Fig. 10. Variation of% removal of the dye against concentration of the dye for a.ZnO /SA and b. ZnO /cmC

Effect of irradiation time

Irradiation time plays an important role in the photocatalytic degradation process of MBdye. Effect of irradiation time with constant dose of the catalyst (50mg/50mL for ZnO / SA and 20mg/50ml for ZnO /cmC) and initial concentration (10ppm) of MB dye has been observed from the Fig.11 a and b, that the percentage of photodegradation increases with increase in irradiation time and complete degradation was obtained within 150 minutes for ZnO / SA and 120 minutes for ZnO /cmC nanocomposites. This may be due to with increase in irradiation time, dye molecules and catalysts have enough time to take part in photocatalytic degradation process and hence percentage of degradation increases (Meenakshi Sundaram *et al.*, 2014; Uma Rajalakshmi and Alagumuthu, 2019; 2021).

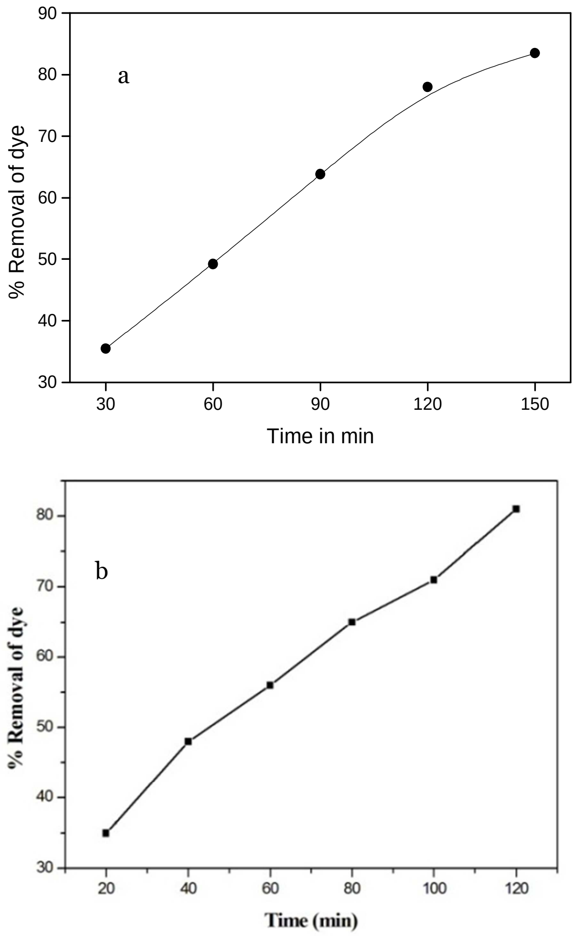

Fig. 11. Variation of% removal of MB dye against irradiation time for a.ZnO / SA and b. ZnO /cmC.

Effect of pH variation

The wastewater from textile industries usually has a wide range of pH values. Further, the generation of hydroxyl radicals is also a function of pH. The pH is varied from 2 to 12 as shown in the Fig 12 a and b the% removal of MB dye is noted. Higher percentage removal occurred at pH 12 because at this basic condition the surface of the catalyst will become negatively charged so the cationic dye (MB) was easily attracted by the catalyst (Uma Rajalakshmi and Alagumuthu, 2019; 2021).

.

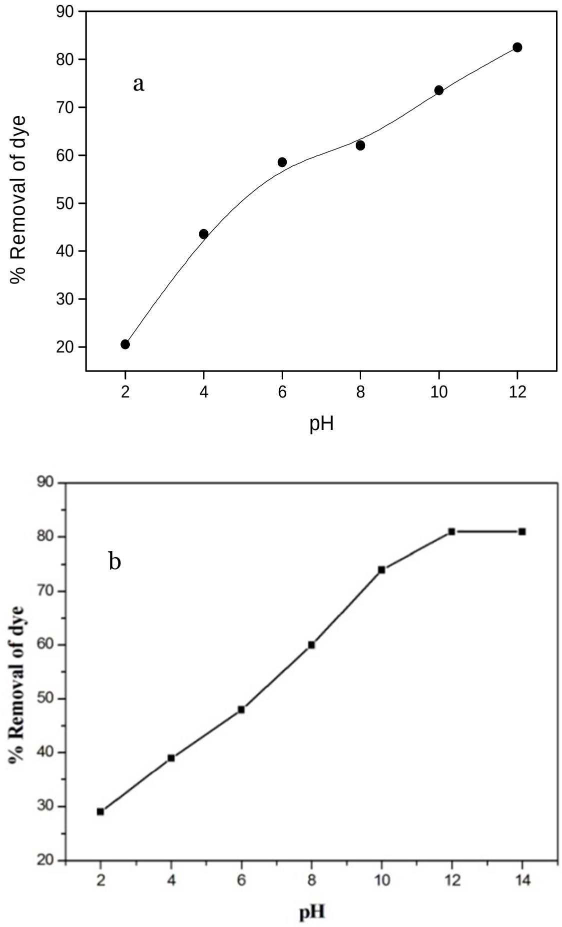

Fig.12. Variation of% removal of MB against pH for a.ZnO / SA and b. ZnO /cmC.

Reuse of catalyst

The reuse of a 50mg of synthesized ZnO / SA nanocomposite and 20mg of ZnO /cmC nanocomposite performed on a 10 ppm (50mL) solution at an optimum pH 12 is performed for four cycles, where the photocatalytic degradation of the nanocomposite was reduced from 82% on the first usage to 81%, 81% and 80% after the second (Uma Rajalakshmi and Alagumuthu, 2019; 2021), third and fourth cycles of reuse for ZnO / SA nanocomposite and 80% on the first usage to 79%,79% and 78% after the second, third and fourth cycles of reuse for ZnO /cmC nanocomposite respectively as shown in Fig 13.

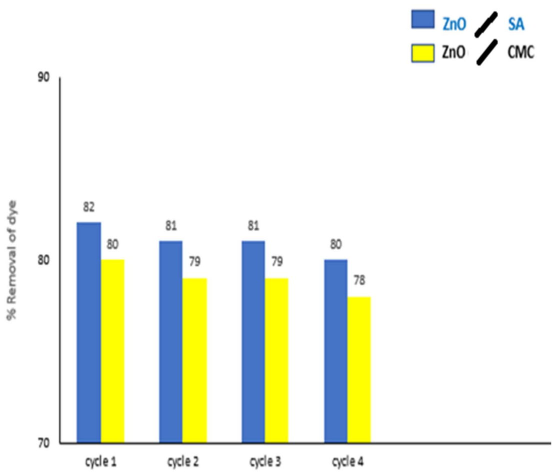

Fig. 13. Reuse of catalyst.

Conclusion

The zinc oxide/sodium alginate and zinc oxide/carboxy methyl cellulose nanocomposites were prepared by a simple precipitation process. The XRD patterns of the synthesized nanocomposites show that the size was approximately 43 nm for zinc oxide/ sodium alginate and 41 nm for zinc oxide/carboxy methyl cellulose nanocomposites From SEM analysis, it is found that the particles are roughly spherical in shape in which the zinc oxide nanoparticles were homogeneously dispersed in the biopolymer matrix. TEM results confirm the zinc oxide nano particles with a mean diameter of 41-45 nm were encapsulated by the biopolymers and hexagonal wurtzite structure of ZnO is confirmed by XRD and TEM. AFM studies reveal uniform surface topology. The FTIR spectrum confirms the functional groups of alginates, carboxy methyl cellulose and zinc oxide. UV-Vis absorption spectra reveal the characteristic absorption of zinc oxide nanoparticles around 330 nm. Photocatalytic activity studies were performed effectively upon MB dye and 82% and 80% removal was achieved respectively at an optimum pH of 12 with catalytic loading of 50mg and 20mg in an initial dye concentration of 10 ppm within 150 minutes and 120 minutes respectively for zinc oxide/sodium alginate and zinc oxide/carboxy methyl cellulose nanocomposites. The nanocomposites also showed excellent reusability even after four cycles of photocatalytic degradation of methylene blue dye. Thus, the synthesised nanocomposites can be effectively applied in waste water treatment to remove dyes.

Reference

Baran W, Makowski A, Wardas W. 2008. The effect of UV radiation absorption of cationic and anionic dye solutions on their photocatalytic degradation in the presence of TiO_2. Dyes and Pigments **76,** 226.

Byrappa K, Subramani AK, Ananda S. Rai KL, Sunitha MH, Basavalingu B, Soga K. 2006. Impregnation of ZnO onto activated carbon under hydrothermal conditions and its photocatalytic properties. Journal of Materials Science **41,** 1355-1362.

Changchunchen, Ping Liu, Chun Hua LU. 2008. Synthesis and characterization of nano-size ZnO powders by direct precipitation method', Chemical Engineering Journal **144,** 509-513.

Changhyun Jin, Sunghoon Park, Hyunsu Kim, Chongmu Lee. 2012. Ultrasensitive multiple networked Ga_2O_3-core/ZnO-shell nanorod gas sensors. Sensors and Actuators B: Chemical **1,** 223-228.

Chen G, Wang Y, Dai G, Zhang F. 2016. Immobilization of flower-like ZnO on activated carbon fibre as recycled photo catalysts. Research on Chemical Intermediates **42,** 8227-8237.

Chen G, Wang Y, Shen Q, Song Y, Chen G, Yang H. 2014. Synthesis and enhanced photocatalytic activity of 3D flowerlike ZnO microstructures on activated carbon fiber. Materials Letters **123,** 145-148.

Dai ZR, Pan ZW, Wang ZL. 2002. Gallium oxide nanoribbons and nanosheets. The Journal of Physical Chemistry B **106,** 902-904.

Dang C, Li ZF, Yang C. 2018. Measuring firm size in empirical corporate finance. Journal of banking & finance **86,** 159-176.

Hagfeldt A, Boschloo JG. 2001. Spectro electrochemistry of nanostructured NiO. The Journal of Physical Chemistry B **15,** 3039-3044.

Hengyu Xu, Chen Qian, Xiaojie Tan, Wei Xia, Yu long WU. 2022. Photocatalytic oxidation for efficient 4-chloro-guaiacol degradation over Co-doped graphitic carbon nitride and the effect of Co-doping concentration on optical properties of carbon nitride. Inorganic Chemistry Communications. **145,** 109958.

Holtz J, Ashe S. 1997. Polymerised Colloidal Crystal Hydrogel Films as Intelligent Chemical Sensing Materials. Nature **389,** 829-832.

Jiang H, Herricks T, Xia Y. 2002. CuO nanowires can be synthesized by heating copper substrates in air. Nano letters **12,** 1333-1338.

Kudo A, Miseki P. 2009. Heterogeneous photocatalyst materials for water splitting. Chem. Soc. Rev **38,** 253.

Lili WU, Youshi WU, Yuanchang SHI, Huiying WEI. 2006. Synthesis of ZnO nanorods and their optical absorption in visible-light region. Rare Metals **1,** 68-73.

Lin HH, Wang CY, Shih HC, Chen JM, Hsieh CT. 2004. Characterizing well-ordered CuO nanofibrils synthesized through gas-solid reactions. Journal of applied physics **95,** 5889-5895.

Liu B, Zheng HC. 2004a. Mesoscale organization of CuO nanoribbons: formation of dandelions. Journal of the American Chemical Society **126,** 8124-8125.

Liu XM, Zhang XG. 2004b. NiO-based composite electrode with RuO_2 for electrochemical capacitors. Electrochimica Acta **2,** 229-232.

Lupan O, Emelchenko GA, Ursaki VV, Chai G, Redkin AN, Gruzintsev AN, Tiginyanu IM, Chow L, Ono LK, Roldan Cuenya B, Heinrich H, Yakimov EE. 2010. Synthesis and characterization of ZnO nanowires for nano sensor applications, Materials Research Bulletin **45,** 1026-1032.

Meenakshi Sundaram M, Sangareswari, Mand Muthirulan P. 2014. Enhanced photocatalytic activity of polypyrrole/TiO_2 nanocomposites for acid violet dye degradation under UV irradiation. Int. J. Innov. Res. Sci. Eng **2,** 420-423.

Melian EP, Díaz OG, Rodríguez JD, Colón G, Araña J, Melián JH, Navío JA, Peña JP. 2009. ZnO activation by using activated carbon as a support: characterisation and photoreactivity. Applied Catalysis A: General **364,** 174-181.

Neppolian B, Choi HC, Sakthivel S, Arabindoo B, Murugesan V. 2002. Solar/UV-induced photocatalytic degradation of three commercial textile dyes. J. Hazard. Mater **89,** 303.

Nuli YN, Zhao SL, Qiu QZ. 2003. Nanocrystalline tin oxides and nickel oxide film anodes for Li-ion batteries. Journal of Power Sources **1,** 113-120.

Pearce CI, Lloyd JR, Guthrie JT. 2003. The Removal of Colour from Textile Wastewater using Whole Bacterial Cells: a review. Dyes and Pigments **58,** 179-196.

Raizada P, Singh P, Kumar A, Sharma G, Pare B, Jonnalagadda SB, Thakur P. 2014. Solar photocatalytic activity of nano-ZnO supported on activated carbon or brick grain particles: role of adsorption in dye degradation. Applied Catalysis A: General **486,** 159-169.

Rauf MA, Shehadeh I, Ahmed A, Al-Zamly A. 2009. Removal of Methylene Blue from Aqueous Solution by Using Gypsum as a Low Cost Adsorbent. World Academy of Science: Engineering and Technology **55,** 608-613.

Redouane Haounati, Hamza Ighnih, Rahime, Eshaghi Malekshah, Said Alahiane, Fadi Alakhras, Eman Alabbadf, Huda Alghamdi, Hassan Ouachtak, AbdelazizAit Addi, Amane Jada. 2023. Exploring ZnO/Montmorillonite photocatalysts for the removal of hazardous RhB Dye: A combined study using molecular dynamics simulations and experiments. Materialtoday Communication **35,** 105915.

Robinson T,mcMullan G, Marchant R, Nigam P. 2001. Remediation of dyes in textile effluent: a critical review on current treatment technologies with a proposed alternative. Bioresource technology **77,** 247-255.

Sobana N, Swaminathan M. 2007. Combination effect of ZnO and activated carbon for solar assisted photocatalytic degradation of Direct Blue 53. Solar Energy Materials and Solar Cells **91,** 727-734.

Thi VHT, Lee BK. 2017. Great improvement on tetracycline removal using ZnO rod-activated carbon fiber composite prepared with a facile microwave method. Journal of hazardous materials **324,** 329-339.

Uma Rajalakshmi T, Alagumuthu G. 2019. Facile Synthesis of ZnONanocomposite by an Alginate Mediated Process and a Case Study for Photocatalytic Degradation of MB Dye. Int J of adv sci res and management **4,** 82-86.

Uma Rajalakshmi T, Alagumuthu G. 2021. Enhanced Role of Biopolymers in the Photo catalysis of Metal oxide/ Biopolymer Nanocomposites upon Methylene blue and Congo red Dyes. Int J of all res edn and sci methods **9,** 121-131.

Vinayagam M, Ramachandran S, Ramya V, Sivasamy A. 2018. Photocatalytic degradation of orange G dye using ZnO/biomass activated carbon nanocomposite. Journal of environmental chemical engineering **3,** 3726-3734.

Yang X, Wang D. 2018a. Photo catalysis: from fundamental principles to materials and applications. ACS Appl Energy Mater **1,** 6657-6693.

Yang Y, Guan C. 2018b. Adsorption properties of activated carbon fiber for highly effective removal of methyl orange dye. In IOP Conference Series: Earth and Environmental Science **208,** 012005.